Molecular basis for insulin fibril assembly

Magdalena I. Ivanova[a], Stuart A. Sievers[a], Michael R. Sawaya[a], Joseph S. Wall[b], and David Eisenberg[a,1]

[a]Howard Hughes Medical Institute, UCLA-DOE Institute for Genomics and Proteomics, Los Angeles CA 90095-1570; and [b]Biology Department, Brookhaven National Laboratory, Upton, NY 11973-5000

Contributed by David S. Eisenberg, September 11, 2009 (sent for review August 7, 2009)

In the rare medical condition termed injection amyloidosis, extracellular fibrils of insulin are observed. We found that the segment of the insulin B-chain with sequence LVEALYL is the smallest segment that both nucleates and inhibits the fibrillation of full-length insulin in a molar ratio–dependent manner, suggesting that this segment is central to the cross-β spine of the insulin fibril. In isolation from the rest of the protein, LVEALYL forms microcrystalline aggregates with fibrillar morphology, the structure of which we determined to 1 Å resolution. The LVEALYL segments are stacked into pairs of tightly interdigitated β-sheets, each pair displaying the dry steric zipper interface typical of amyloid-like fibrils. This structure leads to a model for fibrils of human insulin consistent with electron microscopic, x-ray fiber diffraction, and biochemical studies.

amyloid | fibril structure

One of the roughly 25 disorders categorized as amyloid diseases (1) is injection amyloidosis. In this rare condition, full-length insulin molecules are found in fibrillar form at the site of frequent insulin injections (2–4). These insulin fibrils formed in vivo display the defining characteristics of amyloid aggregates (5), including binding the dye Congo red with "apple-green" birefringence, an elongated, unbranched fibrillar morphology (4), nucleation-dependent polymerization, and the cross-β x-ray diffraction pattern (6–8). Recently, serum samples from patients with Parkinson's disease have been found to display an autoimmune response to insulin oligomers and fibrils (9), possibly indicating the presence of insulin aggregates in this disease as well. Insulin also forms amyloid-like fibrils in vitro, which are promoted by elevated temperatures, low pH, and increased ionic strength (4, 10). In addition, insulin fibril formation has been a limiting factor in long-term storage of insulin for treatment of diabetes. Thus, better understanding of insulin fibrillation could lead to safer handling and more cost-effective storage of insulin.

Because insulin offers the structural simplicity of two short polypeptide chains constrained by one intramolecular and two intermolecular disulfide bonds, models of the structure of insulin fibrils have been numerous. Upon fibrillation, the molecule of insulin undergoes structural changes from a predominantly α-helical state to a β-sheet rich conformation. The fibrillar β-sheets have been described as either parallel (11–13) or antiparallel (14–16). An early model was based on the crystal packing of a despentapeptide insulin molecule (with residues B26–B30 removed) (4, 17). More recently, Jimenez et al. (18) used cryo-electron microscopy images to propose that upon fibril assembly the α-helical insulin molecules undergo conformational transition into a flat β-sheet–rich state. Still more recently, from x-ray solution scattering and ab initio modeling, Vestergaard et al. (19) proposed that insulin fibrils are formed by primarily α-helical oligomers. The first atomic-level view of the interactions between segments of insulin which may be part of fibrillar spine came from single crystal structures of the fibril-forming peptide segments LYQLEN (residues A13–A18) and VEALYL (residues B12–B17) (16).

Previous biophysical studies suggest that the B chain, or a segment of it, may be the primary determinant of insulin fibrillation. For example, equimolar amounts of the peptide RRRRRRLVEALYLV (containing residues B11-B17 of the B chain) can attenuate insulin fibrillation (20). In addition, the point mutations H10D and L17Q in the B chain of insulin prolong the lag phase of insulin fibrillation, further supporting the importance of this segment in fibril formation (21). Also, exposing this fibril-prone segment by truncating the C-terminal five residues of the B chain increases the propensity of insulin for fibril formation (4, 17).

Other studies have shown that the A chain also contributes to insulin fibrillation. Both A chain and B chain can form fibrils on their own (22, 23), and seeds of A chain or B chain can nucleate the fibrillation of full length insulin (22). In addition, it was reported that segments as short as six residues from either A chain (residues A13–A18) or B chain (residues B12–B17) can form fibrils by themselves (24). The same segments from A chain (residues A13–A19) and B chain (residues B9–B19) were found to be protected against hydrogen exchange when insulin was incubated in conditions favorable for fibril formation (25). Based on these findings, it seems that a segment from the A chain may also be involved in the formation of the spine of insulin fibrils.

Much evidence has accumulated in support of the view that only specific segments of amyloidogenic proteins form the spine of amyloid fibrils. Peptide segments, as short as three to four residues, can form fibrils by themselves in vitro (26–30). Furthermore, these segments from the spine of the fibril often act as inhibitors of fibrillation of their parent proteins. For example, prion peptide (residues 113–120) and modified peptides from Aβ (residues 16–20) and IAPP (residues 22–27) can attenuate fibril formation of the full-length protein (31–35).

Our work suggests that the B-chain segment LVEALYL is the main contributor to the spine formation of fibrils of full-length insulin. The crystal structure of the segment LVEALYL provides a molecular view of the structural organization of the spine of insulin fibrils and was used to build a model of fibrils of the full-length protein. The model is supported by the x-ray fiber diffraction of insulin fibrils and scanning-transmission electron microscopy (STEM) analysis of the morphology of insulin fibrils.

Results

Insulin Segments Form Fibrils and Alter Lag Time of Insulin Fibril Formation. The rationale behind our experiments is that segments that form fibrils on their own and alter the rate of fibril formation when co-incubated with full-length protein are likely to participate in the spine of full-length fibrils. Based on previous studies (24), there are two segments of insulin that form fibrils in isolation from the rest of the protein; these are VEALYL from the B chain and LYQLEN from the A chain.

To ascertain whether either or both of these segments form the spine of insulin fibrils, we studied their effects on the rate of

Author contributions: M.I.I., S.A.S., and D.E. designed research; M.I.I., S.A.S., and M.R.S. performed research; M.I.I., M.R.S., and J.S.W. contributed new reagents/analytic tools; M.I.I., S.A.S., and M.R.S. analyzed data; and M.I.I., S.A.S., M.R.S., and D.E. wrote the paper.

The authors declare no conflict of interest.

Data deposition: The coordinates of the crystal structure of LVEALYL have been deposited with the Protein Data Bank, www.pdb.org (PDB ID code 3HYD; structure factors PDB ID code 3HYD-SF).

[1]To whom correspondence should be addressed. E-mail: david@mbi.ucla.edu.

This article contains supporting information online at www.pnas.org/cgi/content/full/0910080106/DCSupplemental.

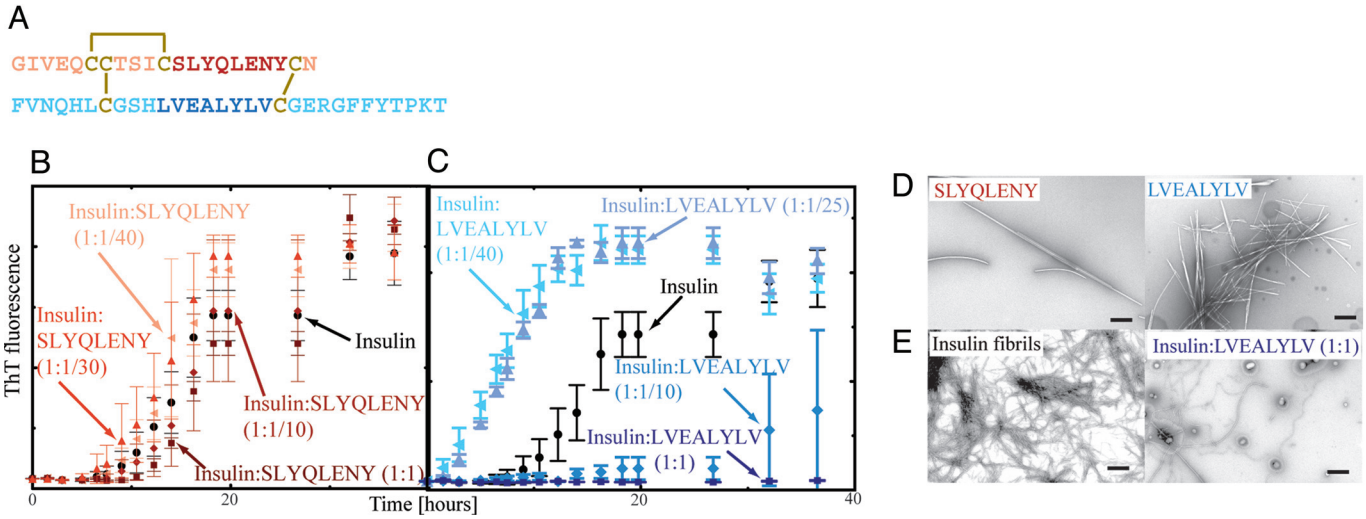

Fig. 1. An eight-residue segment from the insulin B chain accelerates and inhibits insulin fibril formation. (*A*) Amino acid sequence of insulin. Segment SLYQLENY of the A chain is dark red. Segment LVEALYLV of the B chain is dark blue. Disulfide bonds are colored in yellow. (*B*) SLYQLENY of the A chain, when added to the reaction mixture, does not affect the rate of full-length insulin fibril formation. Fibrillation was monitored as a function of time by measuring ThT fluorescence. Full-length insulin starts to form fibrils after 8–10 h, and its conversion is complete in ≈20 h. (*C*) Fibrillation assay showing LVEALYLV from the B chain inhibits insulin fibril formation at a concentration 10 times less than the concentration of insulin. LVEALYLV also accelerates fibril formation when present at concentrations 25–40 times less than the concentration of insulin. Note that neither SLYQLENY (A chain) nor LVEALYLV (B chain) fluoresce in the presence of ThT. All points represent the mean value of at least four replicates, with error bars representing the SD. (*D*) Electron micrographs showing that SLYQLENY and LVEALYL aggregates are fibrillar in morphology (*E*). LVEALYLV in equimolar ratios inhibits insulin fibril formation. Many fibrils were observed in the micrograph of the sample of full-length insulin taken 48 h after the beginning of fibrillation assay (*left*). In contrast, there were only a few fibrils in the sample of insulin incubated at equimolar ratio with LVEALYLV (*right*). (Scale bars, 400 nm.)

fibrillation of full-length insulin. Both of these segments are located between the two interchain disulfide bonds of full-length insulin (Fig. 1*A*). In our first experiments, we tested the effect on insulin fibril formation of nine six-residue segments with sequences spanning the A and B chain segments between the two interchain disulfide bonds of insulin [Supporting Information (SI) Table S1]. None of the nine six-residue segments affected the fibrillation of full-length insulin. These results suggest that the spine of insulin fibrils is longer than six residues.

Searching for the smallest segment of insulin that affects the kinetics of fibrillation of full-length insulin, we synthesized two eight-residue segments: SLYQLENY (A chain) and LVEALYLV (B chain) (Fig. 1*A*). Both SLYQLENY and LVEALYLV form fibrils in solution (Fig. 1*D*). As seen in Fig. 1*B*, the A chain segment SLYQLENY does not affect insulin fibrillation. In contrast, the B chain segment LVEALYLV slows insulin fibrillation when incubated in molar concentrations down to 10 times less than that of insulin (Fig. 1*C*). The strongest inhibitory effect of LVEALYLV is observed when incubated in equimolar concentrations with insulin. The lag time of fibril formation with LVEALYLV at a 1:1 molar ratio is more than 10 times that of insulin alone (Fig. 1*C*). In addition, we observed few fibrils in electron micrographs of the sample of insulin with LVEALYLV (1:1) compared with the densely packed fibrils observed in the sample containing only insulin (Fig. 1*E*). We also observed that LVEALYLV nucleated fibril formation when incubated in molar concentrations 40 times less than insulin (Fig. 1*C*). Thus, depending on the concentrations used, LVEALYLV either inhibits or nucleates fibril formation.

Given that the six-residue segments do not affect the rate of insulin fibril formation and that the eight-residue segment LVEALYLV does, we wanted to know whether either of the two seven-residue peptides within LVEALYLV affected fibril formation. The two seven-residue peptides LVEALYL and VEALYLV formed fibrillar aggregates (Fig. 2*A* and Fig. S1*A*). However, only LVEALYL inhibited fibril formation of full-length insulin (Fig. 2*C* and Fig. S1*B*), and there were only sparse fibrils present in the sample of insulin incubated with LVEALYL (Fig. 2*B*). Also, depending on its molar ratio relative to that of insulin, LVEALYL, like LVEALYLV, either delays or nucleates fibril formation (Fig. 2*C*).

Structure of LVEALYL. The segment LVEALYL forms microcrystals diffracting to 1 Å resolution, and we were able to determine

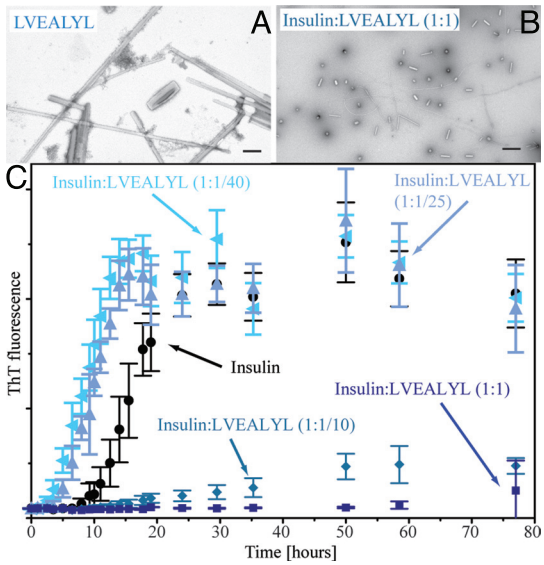

Fig. 2. LVEALYL from B chain is the smallest segment that can alter the rate of insulin fibril formation. (*A*) Electron micrograph of fibrillar aggregates of B-chain LVEALYL. (*B*) Electron micrograph of sample taken from equimolar solution of insulin and LVEALYL after 48 h from beginning of assay. Note that there are only sparse fibril-like aggregates. (*C*) Fibrillation assay showing that B-chain LVEALYL accelerates insulin fibril formation when added to the reaction mixture at low concentrations, but inhibits insulin fibril formation at higher concentrations. (Scale bars, 400 nm.)

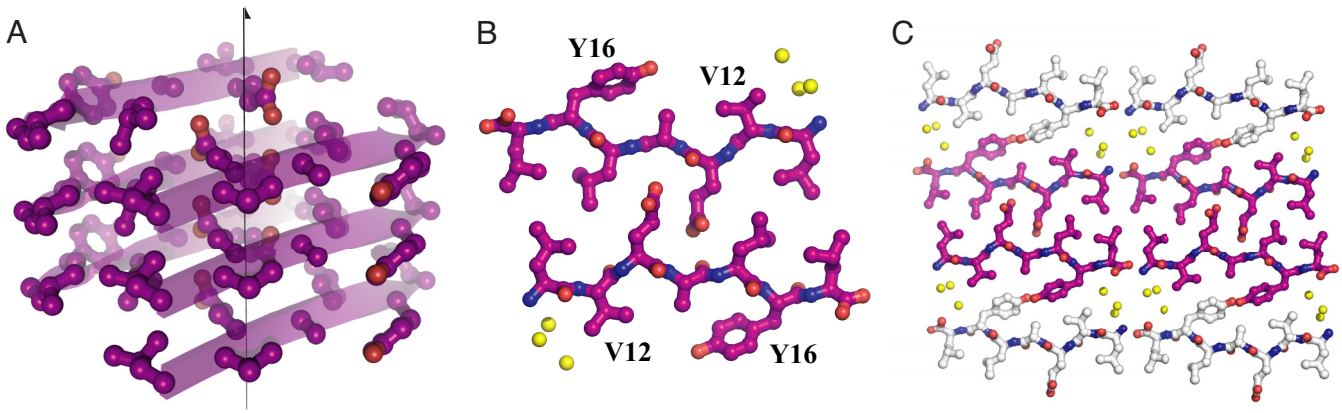

Fig. 3. Atomic structure of B-chain segment LVEALYL, which forms fibril-like microcrystals. (*A*) View perpendicular to fibril axis showing pair of β-sheets formed by LVEALYL molecules. Crystal needle length runs vertical in this orientation. (*B*) View down fibril axis showing one layer of interdigitated pair of LVEALYL molecules, which interlock tightly to form the dry steric zipper interface. Pairs of extended β-strands of LVEALYL are stacked in register upon each other, so this figure may be thought of as a projection of two β-sheets, each containing some 100,000 layers. Note that this dry steric zipper interface is devoid of water molecules (shown in yellow). (*C*) Packing of LVEALYL molecules in crystal, viewed down fibril axis as in (*B*). Molecules forming the dry steric zipper interface are purple and are separated by water molecules from the next sheets in gray. Thus in LVEALYL crystals one side of each sheet faces water molecules (wet interface).

its fibril-like structure. Extended strands of LVEALYL pack in register into parallel β-sheets, which run the entire length of the needle crystal (Fig. 3*A*). Alternating side chains L, E, L, and L extend toward a second, identical β-sheet (Fig. 3*B*). The same set of side chains extending from the second sheet intermesh with those from the first, forming a dry, highly complementary interface of the type termed "steric zipper" (16). Each pair of sheets forming the dry interface packs against two other identical steric zippers, separated by wet interfaces containing six water molecules (Fig. 3*C*). The dry interface of the LVEALYL steric zipper buries a larger surface area and displays higher surface complementarity than does the steric zipper of the structure of VEALYL, which we determined earlier (16).

Mass per Unit Length of Insulin Fibrils. A measurement that tells much about the molecular structure of a fibril is its mass per unit length (MPL), which can be determined by STEM. The STEM observations were made on insulin fibrils grown under the same conditions used in the fibril kinetic assays. The most common MPL values of the narrowest fibrils clustered around a mean of 2.85 $\pm$ 0.35 kDa/Å (Fig. 4*A*). This MPL value of 2.85 $\pm$ 0.35 kDa/Å corresponds well with the value of 2.47 kDa/Å expected for two insulin molecules (Mr = 2 $\times$ 5808 Da) per 4.7 Å rise of an amyloid fibril (2 $\times$ 5.81 kDa/4.7Å = 2.47 kDa/Å). Other common MPL values clustered around two and three times this value, suggesting that these fibrils consist of two and three of the narrowest measured filaments. Also observed was a clustering around an MPL value of about four times that of the narrowest measured filament. As seen in the Fig. 4*B*, the morphologies of the fibrils with different MPLs are quite similar with nearly equal cross-over distances. For example, the cross-over distances of fibrils with MPL values of 2.85 kDa/Å and 5.43 kDa/Å is ≈1,200 Å. This value was used in building our model of insulin fibrils shown in Fig. 5. This cross-over distance of ≈1,200 Å implies that each layer of the steric zipper of the fibril spine is not only separated by 4.7 Å from the layer below but is also rotated by ≈0.71° ([4.7 Å/2400 Å] $\times$ 360°).

Discussion

Insulin Segments Forming the Spine of the Fibril. The work presented here shows that the seven-residue B-chain segment LVEALYL can either delay or accelerate insulin fibril formation in a molar ratio–dependent manner. In equimolar ratios with insulin, LVEALYL inhibits fibrillation, and in much lower concentrations than insulin LVEALYL accelerates it. This dual mode of action of the B-chain segment LVEALYL on insulin fibril formation suggests that this segment is important for the formation of the spine of the insulin fibrils. In contrast, segments from the A chain lack this dual mode of action. The experiments represented in Fig. 1*B* show that the eight-residue A-chain segment SLYQLENY does not affect the rate of insulin fibril formation. Apparently this segment, although bound to the B-chain through two disulfide bonds, is peripheral to the spine. In short, our experiments on fibrillation indicate that the spine

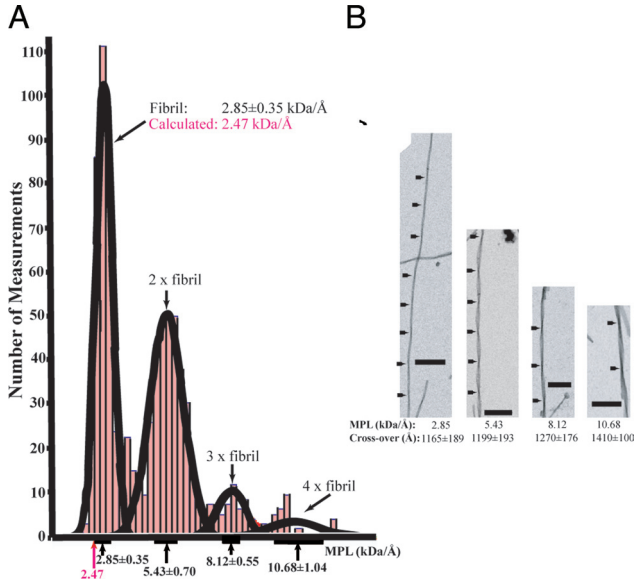

Fig. 4. STEM measurements of MPL of insulin fibrils. (*A*) MPL value of the most abundant fibrils was measured as 2.85 $\pm$ 0.35 kDa/Å, which is comparable to MPL value of 2.47 kDa/Å of the insulin fibril model shown in Fig. 5. The insulin fibril model contains two molecules of insulin per 4.7-Å layer. MPL values of the thicker fibrils correspond to fibrils with four, six, and eight molecules of insulin per 4.7-Å layer. Histogram was produced by using a binning window of 0.25 kDa/Å. (*B*) Electron micrographs of insulin fibrils representing the MPL of the fibril populations shown in (*A*). Note that fibrils with various MPL values display similar morphologies and cross-over distances, suggesting that particles with larger MPL values comprise fibrils with the smallest MPL value of 2.85 kDa/Å. (Scale bars, 100 nm.)

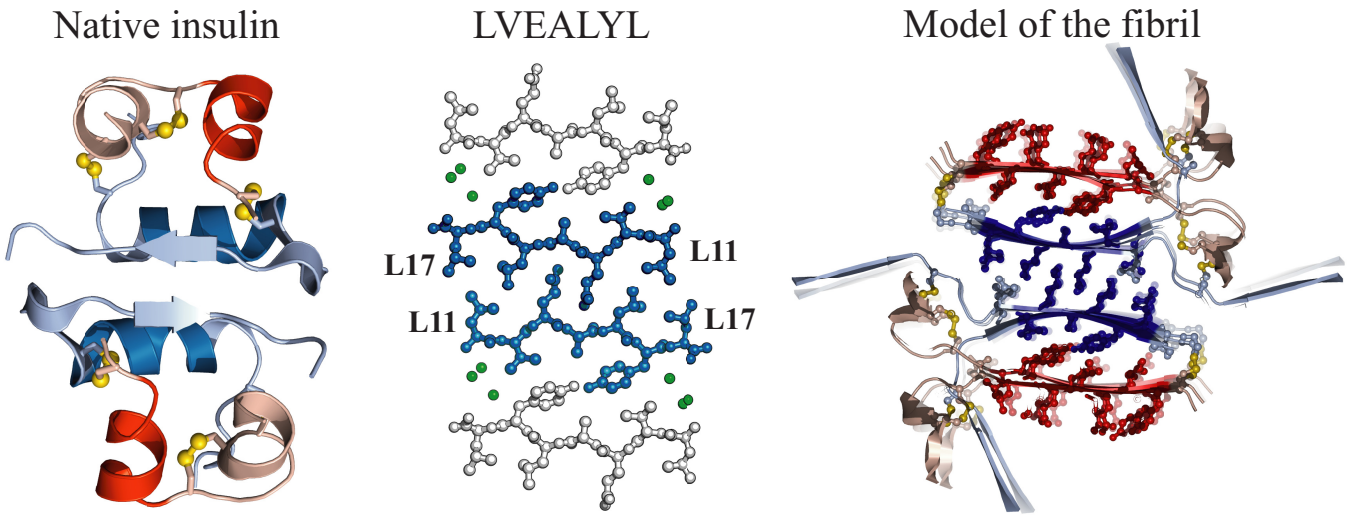

Fig. 5. Fibril model of insulin. (*Left*) Native structure of the insulin dimer (PDB code 1GUJ). A and B chains of insulin molecule are shown in pale red and pale blue, respectively. The LVEALYL segment, which forms the spine of the fibril, is in dark blue. The SLYQLENY segment, from the A chain, which forms auxiliary sheets to the spine of the fibril, is in dark red. Disulfide bonds are shown in yellow. (*Middle*) View down fibril axis of four β-sheets of crystal structure of B chain LVEALYL. The two sheets forming the dry steric zipper interface are in blue. Water molecules are shown as green spheres. (*Right*) View of fibril model, looking down fibril axis. One layer of fibril model is made by stretching both monomers of native insulin (*left*) in a horizontal direction, converting the deep blue helix of the B chain and the deep red helix of the A chain into extended β-strands. These extended β-strands are given the conformations of the four chain segments of the crystal structure shown in the *middle*. Thus the spine of the fibril consists of a dry steric zipper formed by the mating of the central two LVEALYL strands from the B chains of the two insulin molecules, plus two outer strands from the A chains of the two molecules.

of insulin fibrils includes the segment of the B chain between the interchain disulfide bonds, and model building of the fibril was based on this basic observation. In addition, the A chain is covalently bound to the B chain via two interchain disulfide bonds and contributes peripherally to the fibril. The crystal structure of LVEALYL shows how the A chain can be accommodated at the periphery of the spine, as explained below.

Dual Action of LVEALYL on the Rate of Fibrillation. Our observation that the segment LVEALYL is an effective inhibitor of insulin fibrillation, and yet when present in low molar ratios to insulin can accelerate fibril formation, has precedents. In two separate studies, α_1-antichymotrypsin has been observed to both accelerate and inhibit β-amyloid (Aβ) fibrillation. For example, α_1-antichymotrypsin, when incubated with Aβ peptides at ratios lower than 1:100, accelerates Aβ fibrillation (36). However, when the α_1-antichymotrypsin to Aβ1–40 ratio is raised to 1:10, fibril formation is inhibited (37). Apoliprotein E4 (Apo E4) is another example in which fibrillation of Aβ peptide is both inhibited and accelerated. In contrast with LVEALYL and α_1-antichymotrypsin, the apo E4 dual effect on Aβ fibrillation is reversed: Apo E4 inhibits fibrillation when incubated at concentrations lower than those that accelerate fibril formation (36, 38, 39). The dual effect of action of apo E4 and α_1-antichymotrypsin on fibrillation of Aβ was reported in separate studies. This study shows that a short peptide segment can also nucleate and inhibit fibril formation.

The molecular mechanism of the dual effect is unknown. One possibility is that, at low concentrations, LVEALYL nucleates the spine of full-length insulin fibrils more rapidly than do insulin molecules. This is reasonable because the side chains of the segment LVEALYL are exposed, and hence a small group of molecules can interact with each other by intermeshing their side chains, thereby forming a nucleus. In full-length insulin molecules, there must be conformational changes for the LVEALYL side chains of the segment to be exposed and to interact with each other. Once nuclei are formed, full insulin molecules can add to the growing fibril. At high concentrations, LVEALYL can compete for sites on the nucleus with full insulin molecules and can slow fibril growth.

Model for the Insulin Fibril, Based on the LVEALYL Crystal Structure. Taken together, the x-ray fiber diffraction pattern of aligned insulin fibrils and MPL measurements suggest important features of fibrils of full-length insulin. The x-ray fiber diffraction pattern reveals that the fibrils consist of β-sheets running parallel to the fibril axis with their β-strands running perpendicular (13). Thus, the 4.7 Å reflection in the x-ray diffraction pattern (Fig. 6*A*) corresponds to the distance between the strands in the β-sheets. The two broad reflections centered at 11.7 Å and 9.0 Å on the equator (horizontal axis) correspond to the distances between the sheets in the insulin fibril. These two

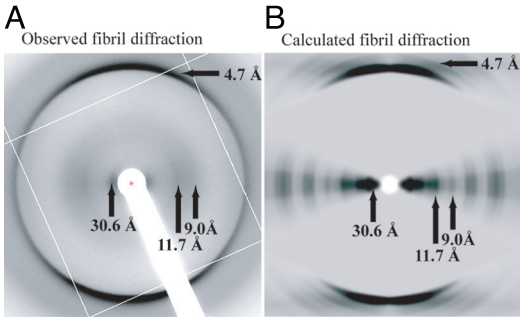

Fig. 6. Comparison ofobserved and calculated fibril diffraction patterns of insulin fibrils. (*A*) Cross-β x-ray diffraction pattern of oriented insulin fibrils. On the meridian (vertical axis), there is one strong reflection at 4.7 Å, corresponding to separation of strands within each β-sheet. The weaker reflections on the equator (horizontal axis) are at 9.0 Å and 11.7 Å, arising from separations between β-sheets. (*B*) Simulated fibril diffraction pattern calculated from the model of the insulin fibril of Fig. 5. An excellent agreement of the diffraction pattern of the model with the observed pattern is noticeable, particularly the 4.7 Å reflection on the meridian and the 9.0 Å and 11.7 Å reflections on the equator.

reflections might imply that there are two pairs of sheets with different sheet-to-sheet distances, which form the fibrils. The MPL measurements suggest that there are two insulin molecules per 4.7 Å along the fibril (Fig. 4*A*).

Based on the findings above, the atomic structure of the B chain segment LVEALYL was used as the molecular basis for the steric zipper spine of the insulin fibril. Insulin fibrils are primarily composed of β-sheets (40), which implies that LVEALYL undergoes a conversion from its native α-helical structure (shown in dark blue in Fig. 5, *left panel*) into an extended β-strand, as in the crystal structure of LVEALYL (shown in dark blue in Fig. 5, *middle panel*). In our insulin fibril model, two strands of LVEALYL from two insulin molecules interdigitate to form one layer of the steric zipper spine of the fibril. Thus, in the fibril of full-length insulin, LVEALYL retains its conformation from the crystal structure (Fig. 5, *right panel*).

The covalent constraints of the disulfide bonds linking the B chain to the A chain (41) force the A chain also to convert to an extended β-strand upon extension of the LVEALYL α-helix of the B chain (Fig. 5, *right panel*). The crystal packing of LVEALYL molecules also provides a structural template for the extended A chain segment LYQLENY. Thus, this A chain segment adopts the backbone conformation of the β-strands (colored in gray Fig. 5, *middle panel*) which lies astride the β-strands forming the dry steric zipper interface. These two outer β-sheets of the spine of insulin fibril are formed by two stacks of LYQLENY segments of the A chain (Fig. 5, *right panel*). The two B chain LVEALYL β-sheets, which form the dry steric zipper interface, lie between the two sheets formed by LYQLENY. Because LYQLENY contains a Tyr residue in the second position, this side chain superimposes on a Tyr from LVEALYL in the crystal structure, preserving the "kissing tyrosine" interaction observed across the wet interface of the crystal of LVEALYL (Fig. 5, *middle panel*) in the fibril model of full-length insulin. These four β-strands complete the model of the fibril spine.

The remaining segments of the A and B chains outside of the fibril spine were modified from their native structure to fit within the constraint of two molecules per 4.7 Å layer. Furthermore, to be compatible with the 1,200 Å cross-over distance observed in insulin fibrils, each layer of our model is given a left-hand twist of $\approx$0.71° with respect to the layer below. The result is the fibril model shown in Fig. 5 (*right panel*).

In summary, the spine of our model contains four β-sheets, the inner pair forming a steric zipper that superimposes on our crystal structure of LVEALYL from the B chain. The outer two β-sheets are formed from the segment LYQLENY of the A chain, also found to contribute to the fibril spine. At the periphery of the model, the N- and C-termini retain the native-like structure of the insulin molecule. A similar model, with a steric zipper spine and native-like structure on the periphery, was proposed for a designed amyloid of ribonuclease A (42).

A comparison of our model with the density of the 3D cryo-EM reconstruction of insulin fibrils, determined by Jimenez et al. (18), is given in Fig. S2. The overall shape of the electron density is captured well in most parts by our model (Fig. S2, *right*). The parts of the model that do not fit the density map are outside the spine of the fibril and possibly disordered, which could explain why they are not observed in the low-resolution density map. Moreover, the calculated MPL of insulin fibrils, including only the residues from the core of the fibrils, is within experimental error of the value obtained by Jimenez et al. (18) (for more details, see SI Text). Thus, we can conclude that our model agrees with the cryo EM density (18).

Assessment of Our Insulin Fibril Model. The model has been built to be consistent with several structural and biochemical observations. First, its structure with two insulin molecules per 4.7 Å layer of the fibril is consistent with our MPL measurements (Fig. 4). It was also found that three dimers of insulin comprise the fibril precursors (43). Thus the fibril growth proceeds via stacking of these precursors along the fibril axis, suggesting that insulin fibrils are formed of dimers repeating along the length of the fibrils in agreement with our MPL measurements. Second, the simulated fiber diffraction pattern (Fig. 6*B*) computed from our model corresponds well to the observed cross-β pattern of oriented insulin fibrils (Fig. 6*A*). Of note, two equatorial reflections, which arise from sheet-to-sheet interactions, are present in both the simulated and observed diffraction patterns at 11.7 Å and 9.0 Å. (Fig. 6). Third, our previous finding that crystals of LVEALYL can accelerate fibril formation of insulin (16) implies that the crystal structure of the peptide resembles the structural organization of the fibril spine. This is the basis for our use of the structure of LVEALYL as a template for the spine of the full-length insulin fibrils. Fourth, the model is consistent with previous findings (4, 17, 20, 21) and our observation that the B chain is important for fibril formation: the B chain forms fibrils independently and can also delay and accelerate fibril formation. Fifth, our model incorporates the LYQLENY segment of the A chain on the periphery of the spine. This is consistent with finding that segments from the A chain (residues A13–A19) and B chain (residues B9–B19) are protected against proton exchange (25). Sixth, inclusion of the Glu residues of LVEALYL and LYQLEN in the spine of our model may explain the more rapid fibrillation of insulin at pH 2.5, where the Glu is expected to be largely uncharged, than at neutral pH, where it carries a negative charge. Thus our model for the insulin fibril is supported by much structural and biochemical data.

Materials and Methods

Polymerization Assays. Insulin was purchased from Sigma-Aldrich. Peptides were purchased from CS Bio and Celtek Bioscience Peptides. Insulin fibrillation assays were performed with 0.25 mM insulin in 50-mM glycine buffer pH 2.5. All reactions were performed with four or more replicates. The progress of the reaction was monitored by ThioflavinT (ThT) fluorescence (for more information, see the SI Text).

Electron Microscopy. For details on EM, see the SI Text.

Crystallization of LVEALVL. Crystals of LVEALYL grew in a hanging drop after mixing 2 μl of 1.82-mM peptide with 1 μl crystallization solution containing 20% MPD/0.1 M sodium citrate pH 5.5 at room temperature.

X-Ray Crystallographic Data Collection and Processing. X-ray diffraction data sets were collected at the Swiss Light Source beamline X10SA, equipped with a MAR CCD detector. Data were collected in 5° wedges at a wavelength of 0.97645 Å using a 5 μm beam diameter. For more details see Table S2 and SI Text.

Preparation of Oriented Samples and X-Ray Diffraction. For details on preparation of oriented samples and x-ray diffraction, see the SI Text

Model Construction. The model of the insulin fibril was built directly from the crystal structure of the segment LVEALYL (insulin B chain residues 11–17). Model building was performed with the graphics program O (44). This crude model was energy minimized using the program CNS (45) with van der Waals, electrostatic, and hydrogen bonding terms (46) (for more details, see the SI Text).

Simulation of Fibril Diffraction. Simulated fibril patterns of fibril models were produced by cylindrical averaging of the single crystal diffraction intensities (for more information, refer to the SI Text).

STEM Sample Preparation and Data Processing. The samples were prepared at the STEM facility at the Brookhaven National Laboratory (for more information, see the SI Text and Figs. S3 and S4).

ACKNOWLEDGMENTS. We thank Drs. Andrew D. Miranker, Lukasz Salwinski, Ruben Diaz-Avalos, and Ivaylo Dinov for discussion; Dr. Martha Simon and Beth Lin of Brookhaven National Laboratory for making STEM measurements and preparing specimens; Dr. Helen Saibil for providing a cryo-EM reconstruction of insulin fibrils; Prof. Ehmke Pohl and the staff at the Swiss Light Source beamline X10SA for assistance in data collection; and the staff at the Advanced Photon Source beamline 24-ID-E. We thank the National Science Foundation, the Department of Energy/Office of Biological and Environmental Research, the National Institutes of Health, and Howard Hughes Medical Institute for support. S.A.S. was supported by a University of California Los Angeles National Science Foundation Integrative Graduate Education and Research Traineeship. BNL STEM is supported by Department of Energy/Office of Health and Environment Research.

1. Westermark P, et al. (2005) Amyloid: Toward terminology clarification. Report from the Nomenclature Committee of the International Society of Amyloidosis. *Amyloid* 12:1–4.
2. Dische FE, et al. (1988) Insulin as an amyloid-fibril protein at sites of repeated insulin injections in a diabetic patient. *Diabetologia* 31:158–161.
3. Storkel S, Schneider HM, Muntefering H, Kashiwagi S (1983) Iatrogenic, insulin-dependent, local amyloidosis. *Lab Invest* 48:108–111.
4. Brange J, Andersen L, Laursen ED, Meyn G, Rasmussen E (1997) Toward understanding insulin fibrillation. *J Pharm Sci* 86:517–525.
5. Westermark P (2005) Aspects on human amyloid forms and their fibril polypeptides. *FEBS J* 272:5942–5949.
6. Astbury WT, Dickinson S (1935) The x-ray interpretation of denaturation and the structure of the seed globulins. *Biochem J* 29:2351–2360.
7. Geddes AJ, Parker KD, Atkins ED, Beighton E (1968) ''Cross-beta'' conformation in proteins. *J Mol Biol* 32:343–358.
8. Sunde M, Blake C (1997) The structure of amyloid fibrils by electron microscopy and x-ray diffraction. *Adv Protein Chem* 50:123–159.
9. Wilhelm KR, et al. (2007) Immune reactivity towards insulin, its amyloid and protein S100B in blood sera of Parkinson's disease patients. *Eur J Neurol* 14:327–334.
10. Ahmad A, Uversky VN, Hong D, Fink AL (2005) Early events in the fibrillation of monomeric insulin. *J Biol Chem* 280:42669–42675.
11. Bouchard M, Zurdo J, Nettleton EJ, Dobson CM, Robinson CV (2000) Formation of insulin amyloid fibrils followed by FTIR simultaneously with CD and electron microscopy. *Protein Sci* 9:1960–1967.
12. Nettleton EJ, et al. (2000) Characterization of the oligomeric states of insulin in self-assembly and amyloid fibril formation by mass spectrometry. *Biophys J* 79:1053–1065.
13. Burke MJ, Rougvie MA (1972) Cross-beta protein structures. I. Insulin fibrils. *Biochemistry* 11:2435–2439.
14. Yu NT, Jo BH, Chang RC, Huber JD (1974) Single-crystal Raman spectra of native insulin. Structures of insulin fibrils, glucagon fibrils, and intact calf lens. *Arch Biochem Biophys* 160:614–622.
15. Turnell WG, Finch JT (1992) Binding of the dye congo red to the amyloid protein pig insulin reveals a novel homology amongst amyloid-forming peptide sequences. *J Mol Biol* 227:1205–1223.
16. Sawaya MR, et al. (2007) Atomic structures of amyloid cross-beta spines reveal varied steric zippers. *Nature* 447:453–457.
17. Brange J, Dodson GG, Edwards DJ, Holden PH, Whittingham JL (1997) A model of insulin fibrils derived from the x-ray crystal structure of a monomeric insulin (despentapeptide insulin). *Proteins* 27:507–516.
18. Jimenez JL, et al. (2002) The protofilament structure of insulin amyloid fibrils. *Proc Natl Acad Sci USA* 99:9196–9201.
19. Vestergaard B, et al. (2007) A helical structural nucleus is the primary elongating unit of insulin amyloid fibrils. *PLoS Biol* 5:e134.
20. Gibson TJ, Murphy RM (2006) Inhibition of insulin fibrillogenesis with targeted peptides. *Protein Sci* 15:1133–1141.
21. Nielsen L, Frokjaer S, Brange J, Uversky VN, Fink AL (2001) Probing the mechanism of insulin fibril formation with insulin mutants. *Biochemistry* 40:8397–8409.
22. Devlin GL, et al. (2006) The component polypeptide chains of bovine insulin nucleate or inhibit aggregation of the parent protein in a conformation-dependent manner. *J Mol Biol* 360:497–509.
23. Hong DP, Fink AL (2005) Independent heterologous fibrillation of insulin and its B-chain peptide. *Biochemistry* 44:16701–16709.
24. Ivanova MI, Thompson MJ, Eisenberg D (2006) A systematic screen of beta(2)-microglobulin and insulin for amyloid-like segments. *Proc Natl Acad Sci USA* 103:4079–4082.
25. Tito P, Nettleton EJ, Robinson CV (2000) Dissecting the hydrogen exchange properties of insulin under amyloid fibril forming conditions: A site-specific investigation by mass spectrometry. *J Mol Biol* 303:267–278.
26. Balbirnie M, Grothe R, Eisenberg DS (2001) An amyloid-forming peptide from the yeast prion Sup35 reveals a dehydrated beta-sheet structure for amyloid. *Proc Natl Acad Sci USA* 98:2375–2380.
27. Lopez de la Paz M, Serrano L (2004) Sequence determinants of amyloid fibril formation. *Proc Natl Acad Sci USA* 101:87–92.
28. Tenidis K, et al. (2000) Identification of a penta- and hexapeptide of islet amyloid polypeptide (IAPP) with amyloidogenic and cytotoxic properties. *J Mol Biol* 295:1055–1071.
29. Reches M, Porat Y, Gazit E (2002) Amyloid fibril formation by pentapeptide and tetrapeptide fragments of human calcitonin. *J Biol Chem* 277:35475–35480.
30. Tjernberg L, Hosia W, Bark N, Thyberg J, Johansson J (2002) Charge attraction and beta propensity are necessary for amyloid fibril formation from tetrapeptides. *J Biol Chem* 277:43243–43246.
31. Tjernberg LO, et al. (1996) Arrest of beta-amyloid fibril formation by a pentapeptide ligand. *J Biol Chem* 271:8545–8548.
32. Findeis MA, et al. (1999) Modified-peptide inhibitors of amyloid beta-peptide polymerization. *Biochemistry* 38:6791–6800.
33. Gilead S, Gazit E (2004) Inhibition of amyloid fibril formation by peptide analogues modified with alpha-aminoisobutyric acid. *Angew Chem Int Ed Engl* 43:4041–4044.
34. Kapurniotu A, Schmauder A, Tenidis K (2002) Structure-based design and study of non-amyloidogenic, double N-methylated IAPP amyloid core sequences as inhibitors of IAPP amyloid formation and cytotoxicity. *J Mol Biol* 315:339–350.
35. Chabry J, Caughey B, Chesebro B (1998) Specific inhibition of in vitro formation of protease-resistant prion protein by synthetic peptides. *J Biol Chem* 273:13203–13207.
36. Ma J, Yee A, Brewer HB, Jr, Das S, Potter H (1994) Amyloid-associated proteins alpha 1-antichymotrypsin and apolipoprotein E promote assembly of Alzheimer beta-protein into filaments. *Nature* 372:92–94.
37. Eriksson S, Janciauskiene S, Lannfelt L (1995) Alpha 1-antichymotrypsin regulates Alzheimer beta-amyloid peptide fibril formation. *Proc Natl Acad Sci USA* 92:2313–2317.
38. Evans KC, Berger EP, Cho CG, Weisgraber KH, Lansbury PT, Jr (1995) Apolipoprotein E is a kinetic but not a thermodynamic inhibitor of amyloid formation: Implications for the pathogenesis and treatment of Alzheimer disease. *Proc Natl Acad Sci USA* 92:763–767.
39. Wisniewski T, Castano EM, Golabek A, Vogel T, Frangione B (1994) Acceleration of Alzheimer's fibril formation by apolipoprotein E in vitro. *Am J Pathol* 145:1030–1035.
40. Nielsen L, Frokjaer S, Carpenter JF, Brange J (2001) Studies of the structure of insulin fibrils by Fourier transform infrared (FTIR) spectroscopy and electron microscopy. *J Pharm Sci* 90:29–37.
41. Nettleton EJ (1998) Ph.D. thesis. (Oxford University, Oxford).
42. Sambashivan S, Liu Y, Sawaya MR, Gingery M, Eisenberg D (2005) Amyloid-like fibrils of ribonuclease A with three-dimensional domain-swapped and native-like structure. *Nature* 437:266–269.
43. Nayak A, Sorci M, Krueger S, Belfort G (2009) A universal pathway for amyloid nucleus and precursor formation for insulin. *Proteins* 74:556–565.
44. Jones TA, Zou JY, Cowan SW, Kjeldgaard M (1991) Improved methods for building protein models in electron density maps and the location of errors in these models. *Acta Crystallogr A* 47:110–119.
45. Brunger AT, et al. (1998) Crystallography & NMR system: A new software suite for macromolecular structure determination. *Acta Crystallogr D Biol Crystallogr* 54:905–921.
46. Fabiola F, Bertram R, Korostelev A, Chapman MS (2002) An improved hydrogen bond potential: Impact on medium resolution protein structures. *Protein Sci* 11:1415–1423.